ELSEVIER

Journal of Nuclear Materials 290–293 (2001) 1002–1008

journal of nuclear materials

www.elsevier.nl/locate/jnucmat

# Impurity behavior in high performance radiative discharges of JT-60U

S. Sakurai [a,*], H. Kubo [a], A. Takenaga [a], N. Asakura [a], H. Tamai [a], T. Ishijima [b], S. Konoshima [a], K. Itami [a], A. Sakasai [a], S. Higashijima [a], T. Sugie [a], JT-60 Team

[a] *Naka Fusion Research Establishment, Japan Atomic Energy Research Institute, 801-1 Mukouyama, Naka-machi, Naka-gun, Ibaraki-ken 311-0193, Japan*

[b] *Nagoya University, Furou-chou, Chikusa-ku, Nagoya-shi, Aichi 464-0814, Japan*

**Abstract**

Transport coefficients of impurities in reversed shear plasmas are evaluated and compared with those in ELMy H-mode plasmas. The diffusivity is significantly reduced (~1/10) at the internal transport barrier. An inward pinch velocity of −3 m/s is also observed at the ITB. The inward pinch velocity increases as charge number of impurity increases. Effects of Ar seeding to the main plasma are investigated in ELMy H-mode. Argon seeding maintain improved confinement $H^{ITER89} = 1.4$, the clear edge pedestal, the radiation fraction of ~80% and the divertor detachment up to 70% of Greenwald limit. Moreover, argon seeding reduces type I ELM frequency less than half, but the heat load of each ELM on the outer target plate does not change. Therefore, the reduction of energy losses due to ELMs probably causes the improvement of edge confinement in Ar seeded cases, though the radiated power inside the separatrix increases. © 2001 Published by Elsevier Science B.V.

*Keywords:* JT-60U; Impurity transport; Argon; ELM

## 1. Introduction

The improved energy confinement in high density and low dilution plasmas is essential for a fusion reactor. The reduction of plasma wall interactions (PWI) is also needed for the reduction of impurity generation and the protection of plasma facing components. The radiation loss enhancement by impurity seeding was investigated for the reduction of heat load on target plates [1–3].

Reversed shear plasmas have an internal transport barrier (ITB) and higher energy confinement than ELMy H-mode plasmas. On the other hand, the effective charge $Z_{eff}$ in reversed shear plasmas is higher than that in ELMy H-mode plasmas as shown in Fig. 1. An equivalent fusion gain ($Q_{DT}^{eq}$) of 1.25 was obtained with a W-shaped divertor configuration in JT-60U [4]. The $Z_{eff}$ is evaluated by bremsstrahlung measurement and the result of transport analysis agreeing with neutron yield. The reduction of $Z_{eff}$ from 3.5 to 3.2 largely contributed to the progress from $Q_{DT}^{eq} = 1.05$ in open divertor configuration.

The clarification of the impurity transport at the ITB is important for the reduction of dilution. Therefore, transport coefficients of impurities in reversed shear plasmas have been evaluated and compared with those in ELMy H-mode plasmas. An inward pinch velocity at the ITB has dependence the ion charge number of impurity. Impurity transport is summarized in Section 2. More detailed information about this subject is described in [5,6].

ELMy H-mode is adopted as a standard operation mode in ITER-FEAT. The improved confinement $HH = 1.0$, the low dilution $Z_{eff} < 1.8$ and the reduction of PWI should be satisfied simultaneously at 85% of

* Corresponding author. Tel.: +81-29 270 7342; fax: +81-29 270 7449.

*E-mail address:* sakurais@fusion.naka.jaeri.go.jp (S. Sakurai).

0022-3115/01/$ - see front matter © 2001 Published by Elsevier Science B.V.
PII: S0022-3115(00)00475-X

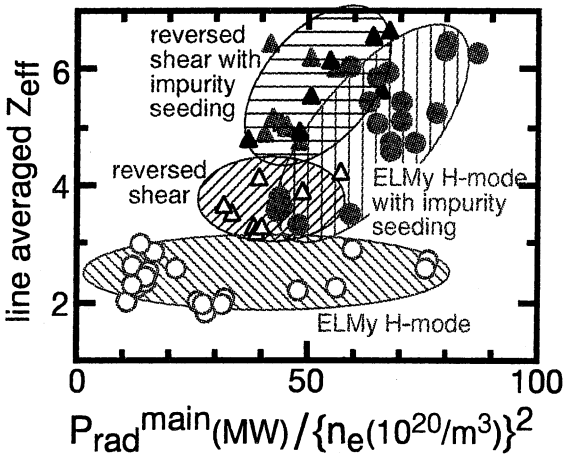


Fig. 1. Line averaged effective charge $Z_{eff}$ vs. radiation power from the main plasma normalized by square of line averaged electron density. Triangles and circles show the cases of reversed shear plasma and ELMy H-mode plasma, respectively. Open symbols show $D_2$ fueled and without gas fueled cases. Closed symbols show impurity seeded cases. $I_p = 0.9$ MA, $B_T = 3.5$ T, $P_{NB} = 8$–15 MW for reversed shear plasmas, and $I_p = 1.2$ MA, $B_T = 2.5$ T, $P_{NB} = 17$–21 MW for ELMy H-mode plasmas.

Greenwald limit density ($n^{GW}$) for ITER-FEAT. These conditions have been mostly achieved simultaneously in ELMy H-mode plasmas with puff and pumped radiative divertor plasma of DIII-D [1]. However, it has not been demonstrated in large tokamaks such as JT-60U [7] and JET [8], because energy confinement degrdaes at high density region. On the other hand, the radiative improved (RI) mode was obtained in TEXTOR-94 [9] and DIII-D [10] by seeding argon or neon to the main plasma, which is characterized by peaked density profile and improved confinement near and above the Greenwald density limit. Therefore, effects of impurity seeding on the energy confinement in ELMy H-mode plasmas should be investigated to improve the confinement at high density.

From the viewpoint of the reduction of PWI, the radiative divertor plasma induced by impurity seeding to the divertor plasma is effective to reduce the steady-state heat load on the target plates between ELMs [1–3]. The particle and impurity exhaust by ELM is also effective to reduce dilution. Nevertheless, results of JET and DIII-D [11] predict that about 30% of pedestal energy will be lost at each ELM. Such a large heat pulse causes unacceptable erosion of target plates. On the other hand, impurity seeding also affects ELM frequency [12].

The radiation enhancement by argon seeding to the main plasma was tried to reduce PWI with maintaining improved confinement at high density in JT-60U. Effects of argon seeding to the main plasma on energy confinement and PWI are described in Section 3.

## 2. Impurity transport in reversed shear plasma [5,6]

### 2.1. Evaluation of transport coefficients by gas-puffing modulation

The gas-puffing modulation experiments using helium and neon were performed in reversed shear and ELMy H-mode plasmas with a plasma current of $I_p = 1.0$ MA, toroidal magnetic field of $B_T = 2.1$ T and the absorbed neutral beam power of $P_{abs} = 7 \sim 11$ MW. The confinement improvement $H^{ITER89}$ was 1.9 in reversed shear plasmas and 1.4 in ELMy H-mode plasmas, respectively. The puffing rate of impurity gas was modulated as a square wave at 2 Hz. The time evolution of helium and neon density profile was measured by charge exchange recombination spectroscopy (CXRS) at 20 radial positions.

The time evolution of helium and neon density at each position was weakly modulated at the frequency of gas-puffing modulation. An amplitude and a phase delay of modulated component are evaluated by least-squares fitting. Furthermore, particle diffusivity $D$ and convection velocity $v$ are evaluated from the amplitude and phase delay in density modulation. The detailed procedure is described in [5].

Radial profiles of the particle diffusivity and the convection velocity of helium and neon are shown in Figs. 2 and 3, respectively. The diffusivity is significantly reduced ($\sim$1/10) at the ITB region in reversed shear plasmas. An inward pinch velocity of $-3$ m/s is also observed at the ITB region.

### 2.2. Dependence of transport coefficients on ion charge number Z

Transport coefficients of helium, carbon and neon impurities have been compared. Diffusivity and convection velocity at the ITB region in reversed shear plasmas and at $r/a = 0.5$ in ELMy H-mode plasmas are plotted as a function of charge number $Z$ in Fig. 4. Carbon is a dominant impurity and it is difficult to separate the modulated component from the background when modulated methane gas-puffing is applied. Therefore, transport coefficients of carbon in reversed shear plasma were evaluated from the time evolution of carbon density profile.

The diffusivity seems to be independent of charge number $Z$, but significantly reduced ($\sim$1/10) at the ITB region in reversed shear plasmas. On the contrary, the inward pinch velocity increases as $Z$ increases. These evaluated values are consistent with preliminary

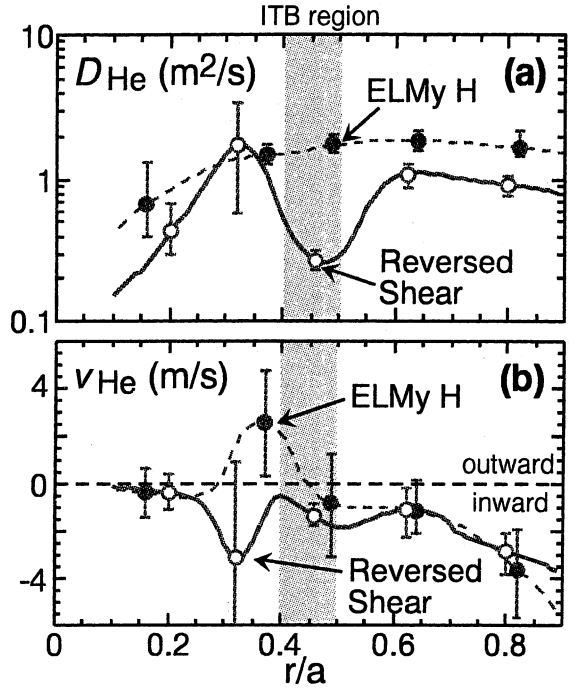


Fig. 2. [3] Radial profiles of the evaluated particle diffusivity $D$ and convection velocity $v$ for helium impurity. Open and closed circles show reversed shear and ELMy H-mode cases, respectively.

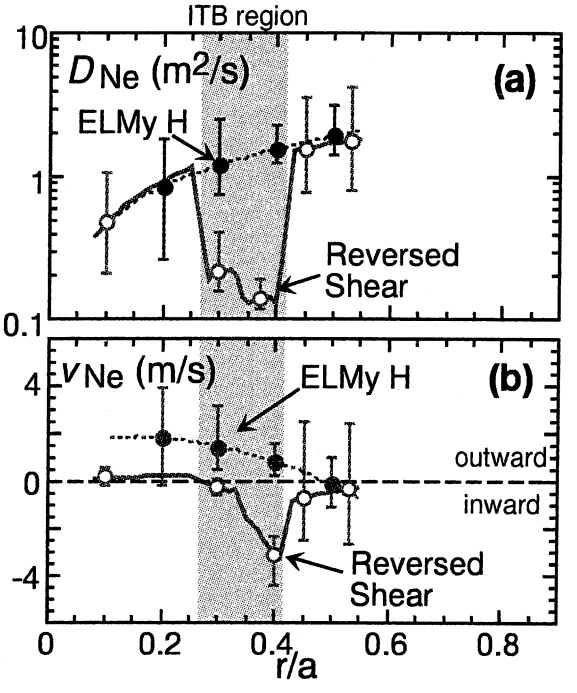


Fig. 3. [3] Radial profiles of the evaluated particle diffusivity $D$ and convection velocity $v$ for neon impurity. Open and closed circles show reversed shear and ELMy H-mode cases, respectively.

prediction by neoclassical transport model within a factor of 2 for helium and carbon.

## 3. Radiation enhancement experiments with argon seeded ELMy H-mode plasma

### *3.1. Experimental setup and comparison between argon seeding and $D_2$ fueling*

Radiation enhancement experiments were carried out by applying weak argon seeding and moderate $D_2$ fueling to the main plasma in ELMy H-mode with neutral beam power $P_{NB} = 17 \sim 21$ MW, $I_p = 1.2 \sim 1.7$ MA, $B_T = 2.5 \sim 3.5$ T and high triangularity ($\delta \sim 0.35$) configuration shown in Fig. 5.

An outer pumping slot was opened between a dome and an outer target plate in 1999. Effective pumping throughout increased from 13 to 16 $m^3/s$ by both-side pumping. Moreover, the outer pumping can exhaust particles through outer divertor for high triangularity configuration as shown in Fig. 5, in which inner strike point is too far from the inner slot for pumping.

Typical wave forms of argon seeded and only $D_2$ fueled cases are compared in Fig. 6. The target plasma conditions were $P_{NB} = 17$ MW, 1.2 MA, $B_T = 2.5$ T, $q_{95} \sim 3.3$ ($q_{eff} \sim 4.0$) and confinement improvement $H^{ITER89}$ was $1.6 \sim 1.8$ at the density of $\sim 0.45 n^{GW}$. Argon gas was seeded at the density of $\sim 0.45 n^{GW}$.

The top and second boxes of Fig. 6 show the fraction of total radiated power $P_{rad}^{total}$ and radiated power from the main plasma $P_{rad}^{main}$ to the net heating power $P_{net} \cdot P_{rad}^{main}$ includes radiation losses inside the separatrix and scrape-off layer (SOL) around the main plasma. In the argon seeded case, the fraction of $P_{rad}^{main}$ enhanced from ~20% to ~40%, and then it exceeded 50% and caused radiative collapse after 8.5 s. The stored energy $W^{dia} > 2$ MJ and $H^{ITER89} = 1.4$ were also maintained up to $\sim 0.7 n^{GW}$. Effects on radiation, edge pedestal, energy confinement and ELM activity are described in Sections 3.2–3.4.

### *3.2. Radiation enhancement and comparison between low and high toroidal field cases*

The fraction of total radiation losses to the net heating power in low toroidal field ($B_T = 2.5$ T) is plotted against the normalized density in Fig. 7(a). The radiation fraction reaches ~80% of heating power in argon seeded cases. The large radiation fracion and divertor detachment can be steadily maintained by using feedback control of radiated power from main plasma

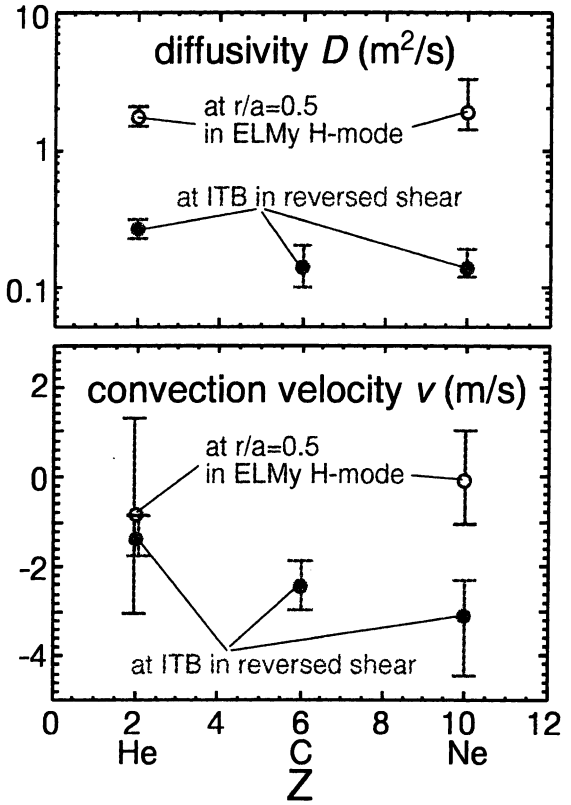


Fig. 4. The dependence of the diffusivity and convection velocity on charge number $Z$ at the ITB region. Open corcles show the values at $r/a = 0.5$ in ELMy H-mode plasmas and closed one shows the value at the ITB in reversed shear plasmas.

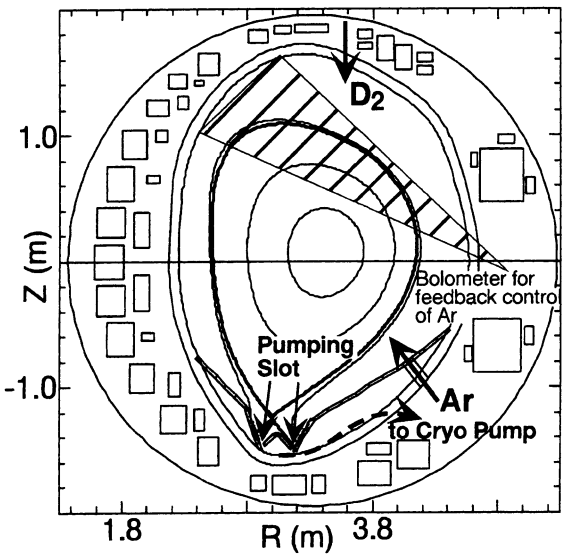


Fig. 5. Experimental setup and plasma configuration of argon seeded ELMy H-mode. Hatched zone shows the sight lines of bolometer for radiated power feedback control by argon puffing rate.

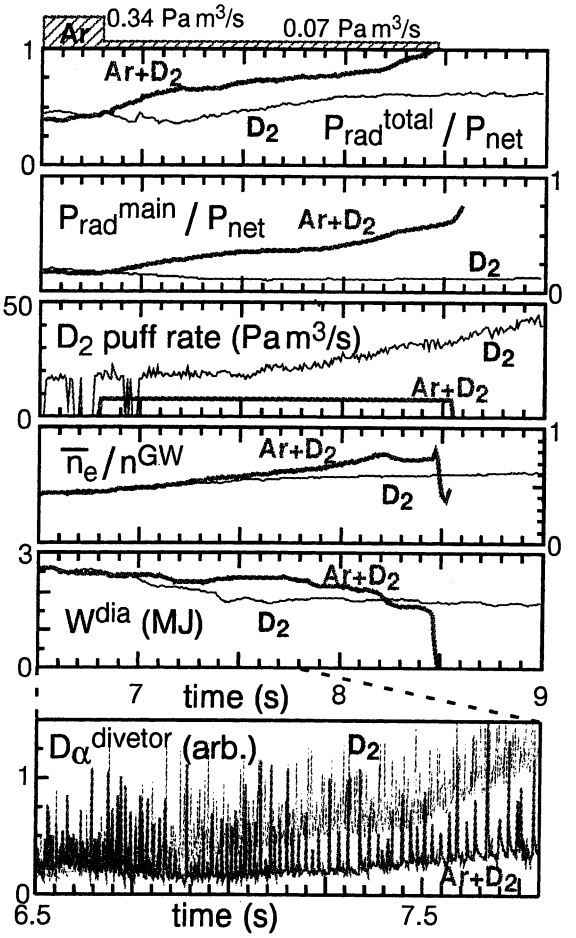


Fig. 6. Typical wave forms of argon seeded and strongly $D_2$ fueled cases. Thick and thin lines show the argon seeded case and the strongly $D_2$ fueling case, respectively. The line averaged electron density normalized by Greenwald limit and the stored energy $W^{dia}$ are shown in the fourth and fifth boxes, respectively.

while improved confinement is maintained, because $P_{rad}^{main}$ increases linearly with argon puffing rate. The radial profile of radiated power shown in Fig. 7(b) indicates argon enhances edge ($0.7a \sim a$) radiation more than several times. However, total radiation losses inside the separatrix remain $\leqslant 30\%$ of absorbed heating power. Therefore, radiative mantle does not degrade energy confinement significantly.

On the other hand, radiation losses in the SOL and the divertor are mainly enhanced in high toroidal field ($B_T = 3.5$ T, $q_{95} \sim 4.7$). However, the electron density and the radiation loss inside the separatrix hardly increase in high $B_T$ cases. Since the high toroidal field and safety factor make the SOL thick and high temperature, the fueling efficiency for $D_2$ and argon gases are probably reduced. Nevertheless, ELMs and the edge pedestal

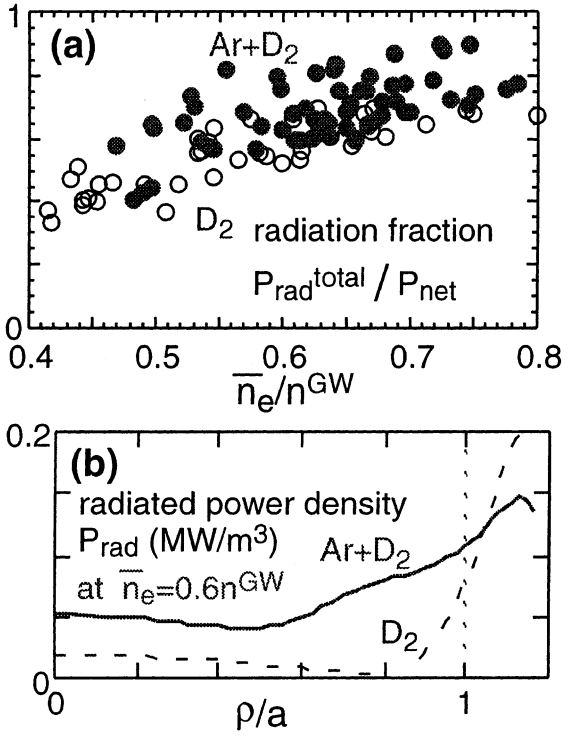


Fig. 7. (a) Radiation fraction of total radiated power to the net heating power vs. line averaged electron density normalized by Greenwald limit. Solid and open circles show argon seeded and strongly $D_2$ fueled cases, respectively. (b) Radial profile of radiated power density at $0.6n^{GW}$ [14]. Plasma conditions were the same as those of Fig. 6.

lose when argon penetrates into the main plasma and enhances radiated power inside the separatrix. Therefore, argon concentration and radiation losses can be hardly controlled in high $B_T$ cases.

### 3.3. Effects on the pedestal temperature and the global energy confinement

Radial profiles of electron density and ion temperature in the argon seeded and the strongly $D_2$ fueled cases are compared in Fig. 8(a). Electron density profiles are flat and similar in both cases. However, the ion temperature in the argon seeded case is higher than in strongly $D_2$ fueled case. Since stiff temperature profiles, which are the evidence for an edge–core relationship, have been also observed in $D_2$ fueled cases [13], it has not been clear that high center temperature in the argon seeded case is caused by confinement improvement at the core region such as RI-mode. On the contrary, the improvement of edge temperature seems to be related to the ELM activity which is affected by argon seeding as described in Section 3.4.

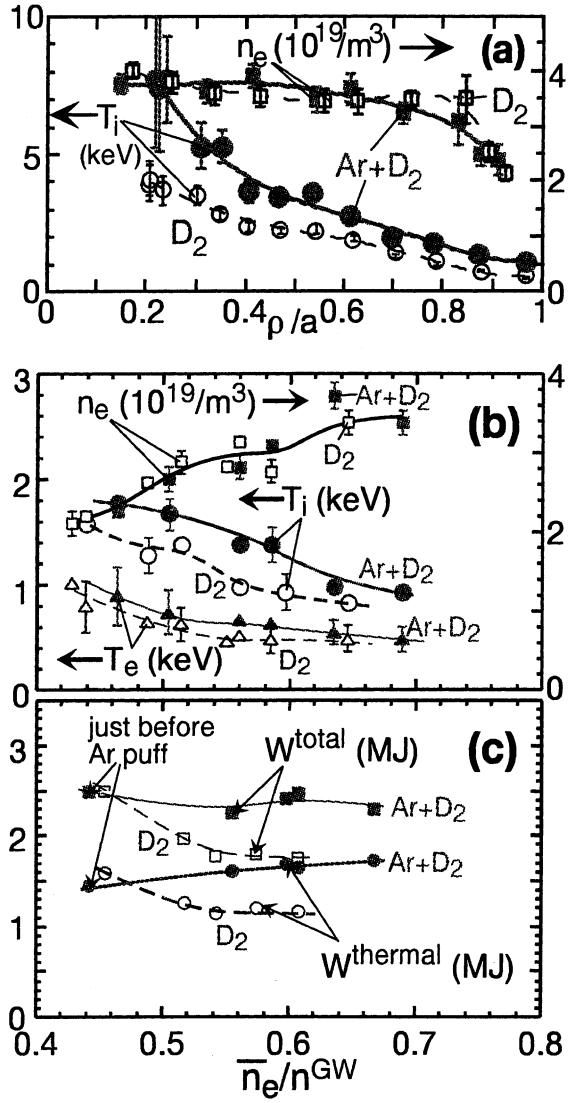


Fig. 8. (a) Radial profiles of ion temperature $T_i$ and electron density $n_e$ at $0.6n^{GW}$ [14]. Plasma conditions were the same as those of Fig. 7(b). (b) Ion and electron temperature $T_i$, $T_e$ and electron density $n_e$ at the pedestal are plotted against the normalized density. (c) The total and thermal components of stored energy vs. normalized density.

The ion temperature profile at the edge pedestal in other discharges was also measured under similar plasma conditions. Ion and electron temperature and electron density at the edge pedestal are plotted against normalized density in Fig. 8(b). The argon seeded case shown by solid symbols indicates smaller degradation of edge ion temperature. On the other hand, not only the height but also the width of pedestal decreases in the strongly $D_2$ fueled case.

The thermal component of stored energy has been evaluated from the result of transport analysis which

agrees with measured temperature and density profiles and neutron yield. Improvement in the total stored energy is mainly caused by the improvement of thermal energy confinement as shown in Fig. 8(c).

### 3.4. Effect on ELM activity

Argon seeding extends the period between each ELM more than twice as shown in the bottom box of Fig. 6. On the contrary, strong $D_2$ fueling increases ELM frequency. These tendencies are consistent with the observation in an Ne seeded ASDEX-U plasma [12].

The surface temperature of target plates has been measured by IRTV with the sampling time of 250 μs. The heat load of each ELM on the outer target plate is evaluated from the time evolution of the temperature profile and is plotted as a function of the ELM frequency in Fig. 9. It does not change significantly when the frequency is divided by 3. Therefore, the energy loss toward the outer target due to ELMs decreases by a factor of 3. On the inner target plate, the peak temperature at some ELMs exceeded measurable range of IRTV and the heat load of each ELM cannot be completely evaluated. Therefore, it should be noticed that the following discussion is limited on outer target plate now. The reduction of the energy loss due to ELM probably causes the improvement of edge temperature in argon seeded caes, though the radiated power inside the separatrix increases.

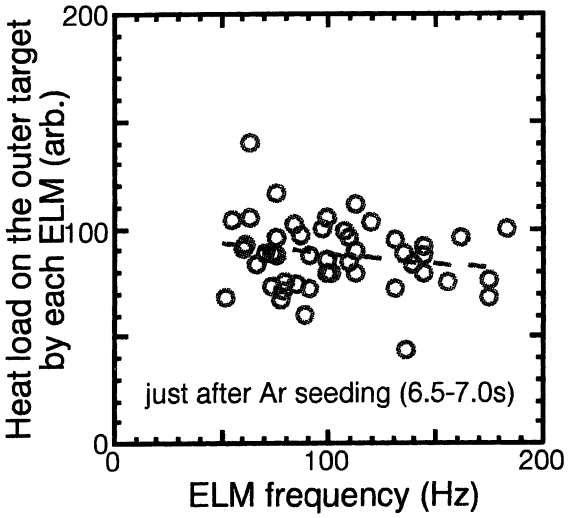


Fig. 9. The heat load on the outer target plate by each ELM is plotted as a function of the ELM frequency. The absolute value of the heat load cannot be evaluated now, because the thermal conductivity of carbon tile surface has large uncertainty. ELM frequency rapidly reduced form ~150 to ~60 Hz during 0.5 s just after argon seeding.

## 4. Conclusion

Transport coefficients of impurities in reversed shear plasmas have been evaluated and compared with those in ELMy H-mode plasmas. The diffusivity is significantly reduced (~1/10) at the ITB region in reversed shear plasmas. An inward pinch velocity of −3 m/s is also observed at the ITB region. The inward pinch velocity increases for higher $Z$ impurities.

Advanced operation scenarios with the ITB such as reversed shear plasmas are attractive for its high energy confinement, but the improved particle confinement at the ITB most likely caused impurity accumulation especially for high $Z$ impurities such as a metal and seeded argon for radiation enhancement. Therefore, the particle transport at the ITB should be controlled to reduce the dilution.

The effect of argon seeding to the main plasma has been investigated in ELMy H-mode plasmas. The radiation fraction of ~80% and the divertor detachment can be steadly maintained by using feedback control of radiated power from the main plasma in $B_T = 2.5$ T. Improved confinement $H^{ITER89} = 1.4$ and the clear edge pedestal are maintained up to $0.7n^{GW}$ by argon seeding.

The radiation losses are enhanced at not only in the divertor but also in the edge plasma ($\geqslant 0.7a$) and the SOL. Nevertheless, the total radiated power inside the separatrix remains $\leqslant$30% of the total absorbed heating power before the confinement improvement loses at $>0.7n^{GW}$ in $B_T = 2.5$ T. On the other hand, the edge pedestal and ELMs lose when argon penetrates into the main plasma and enhances radiated power inside the separatrix in $B_T = 3.5$ T.

Argon seeding maintains high plasma temperature in the main plasma up to $\sim 0.7n^{GW}$, but clearly peaked density profile such as RI-mode has not been observed yet. Since high center temperature has also been observed in only $D_2$ fueled cases when edge temperature is high, it has not been clear that high center temperature in the argon seeded case is caused by confinement improvement at the core region due to seeded argon. Transport analysis including argon seeding effect on ion temperature gradient (ITG) mode is in progress under the collaboration with Princeton Plasma Physics Laboratory.

On the other hand, the high edge temperature is maintained at high density by argon seeding in contrast to the low and narrow edge pedestal in strongly $D_2$ fueled cases. Argon seeding extends the period between each type I ELM more than twice. On the contrary, strong $D_2$ fueling increases ELM frequency and changes ELM from type I to type III. The heat load of each ELM on the outer target plate does not change when the ELM frequency decreases by argon seeding. Therefore, the reduction of energy losses toward the outer target due to ELMs probably causes the improvement of edge

temperature in argon seeded cases, though the radiated power inside the separatrix increases.

Improvement of energy confinements time (~30%) and temperature (~40%) by argon seeding has an advantage, though peaked density profile is not obtained and deuterium density decreases ~15%. Averaged heat load on the target including ELM heat pulse is reduced by radiation enhancement, but the heat load due to each ELM remains large. Therefore, the optimization of energy confinement, dilution and ELM activity should be investigated now.

## Acknowledgements

The authors would like to thank Drs M. Shimada and Y. Miura for useful discussion.

## References

[1] M.R. Wade et al., J. Nucl. Mater. 266–269 (1999) 44.
[2] G.F. Matthews et al., J. Nucl. Fus. 39 (1999) 1097.
[3] K. Itami et al., J. Nucl. Mater. 266–269 (1999) 1097.
[4] K. Fujita et al., Nucl. Fus.. 39 (11Y) (1999) 1627.
[5] H. Takenaga et al., J. Plasma Fus. Res. 75 (1999) 952.
[6] H. Takenaga et al., Nucl. Fus. 39 (11Y) (1999) 1919.
[7] N. Asakura et al., J. Nucl. Mater. 266–269 (1999) 182.
[8] G.C. Vlases et al., J. Nucl. Mater. 266–269 (1999) 160.
[9] B. Unterberg et al., J. Nucl. Mater. 266–269 (1999) 75.
[10] G.L. Jackson et al., J. Nucl. Mater. 266–269 (1999) 380.
[11] T.H. Osborne et al., Plasma Phys. Control. Fus. 40 (1998) 845.
[12] W. Suttrop et al., Plasma Phys. Control. Fus. 40 (1998) 771.
[13] H. Urano et al., Plasma Phys. Control. Fus., submitted.
[14] S. Ide, The JT-60 Team, Phys. Plasma 7 (2000) 1927.